Journal of Structural Biology **126,** 1–15 (1999)
Article ID jsbi.1999.4089, available online at http://www.idealibrary.com on IDEAL®

Correlated Atomic Force and Transmission Electron Microscopy of Nanotubular Structures in Pulmonary Surfactant

Kaushik Nag,* James G. Munro,† Stephen A. Hearn,‡ Johan Rasmusson,† Nils O. Petersen,† and Fred Possmayer*,[1]

*Department of Obstetrics & Gynecology and †Department of Biochemistry and Chemistry, University of Western Ontario, London, Ontario, Canada N5X 2L9; and ‡Department of Pathology, St. Joseph Hospital, London, Ontario, Canada N6A 4V2

Received September 23, 1998, and in revised form January 7, 1999

Pulmonary surfactant stabilizes the lung by reducing surface tension at the air–water interface of the alveoli. Surfactant is present in the lung in a number of morphological forms, including tubular myelin (TM). TM is composed of unusual 40 × 40 nm square elongated proteolipid tubes. Atomic force microscopy (AFM) was performed on polymer-embedded Lowicryl and London Resin-White (LR-White) unstained thin sections. AFM was used in imaging regions of the sections where TM was detected by transmission electron microscopy (EM) of corresponding stained sections. Tapping- and contact-mode AFM imaging of the unstained sections containing TM indicated a highly heterogeneous surface topography with height variations ranging from 10 to 100 nm. In tapping-mode AFM, tubular myelin was seen as hemispherical protrusions of 30–70 nm in diameter, with vertical dimensions of 5–8 nm. In contact-mode AFM and with phase imaging using a sharper (>10 nm nominal radius) probe, square open-ended tubes which resembled typical electron micrographs of such regions were observed. The cross-hatch structures observed inside the tubes using EM were not observed using AFM, although certain multilobe structures and topographic heterogeneity were detected inside some tubes. Other regions of multilamellar bodies and some regions where such bilayer lamella appear to fuse with the tubes were found in association with TM using AFM. EM of acetone-delipidated tubes in LR-White revealed rectangular tubular cores containing cross-hatched structures, presumably protein skeletons. AFM surface topography of these regions showed hollow depressions at positions at which the protein was anticipated instead of the protrusions seen in the lipid-containing sections. Gold-labeled antibody to surfactant protein A was found associated somewhat randomly within the regions containing the protein skeletons. The topography of the gold particles was observed as sharp peaks in contact-mode AFM. This study suggests a method for unambiguous detection of three-dimensional nanotubes present in low abundance in a biological macromolecular complex. Only limited detection of proteins and lipids in surfaces of embedded tubular myelin was possible. EM and AFM imaging of such unusual biological structures may suggest unique lipid–protein associations and arrangements in three dimensions.

Key Words: **tubular myelin; surfactant proteins; surface topography; resin embedding; epitope protrusions; immunogold labeling.**

INTRODUCTION

Pulmonary surfactant is a lipid–protein complex which maintains lung stability by reducing surface tension. Surfactant is secreted by alveolar type II cells in the form of multiple bilayer structures called lamellar bodies (LB). LB undergo transformations in the alveolar fluid to form unusual closely packed arrays of square-shaped elongated nanotubes called tubular myelin (TM) (Weibel and Gil, 1968; Goerke and Clements, 1979; Hawgood, 1997). Surfactant lines the alveolar air–fluid interface with surface-active films, which prevent alveolar collapse at end expiration (Goerke and Clements, 1979; van Golde *et al.*, 1994). Since most of the TM is associated with the alveolar fluid surface it is presumed to be the precursor of the surface-active films. Recently TM structures were found to occur in type II cell cultures only when the extracellular fluid surface was exposed to air (Dobbs *et al.*, 1997).

Pulmonary surfactant collected by lavage consists mainly of lipids such as dipalmitoylphosphatidylcholine (DPPC), phosphatidylglycerol (PG), and small

[1] To whom correspondence should be addressed at the Department of Obstetrics & Gynecology, London Health Sciences Center–University Campus, University of Western Ontario, 339 Windermere Road, London, Ontario, Canada N6A 5A5. Fax: (519) 663-3388. E-mail: fpossmay@julian.uwo.ca.

1047-8477/99 $30.00

amounts of the surfactant-associated proteins (SP-) SP-A, SP-B, SP-C, and SP-D (see Johansson and Curstedt, 1997; Possmayer, 1997; for recent reviews). TM can be reconstituted *in vitro* using DPPC and PG and the surfactant apoproteins SP-A and SP-B, under the influence of millimolar concentrations of calcium (Efrati *et al.*, 1987; Suzuki *et al.*, 1989; Williams *et al.*, 1991). TM is found in low abundance (5–10%) in the surfactant macromolecular complex and is sometimes difficult to detect and characterize, even in reconstituted systems (Williams *et al.*, 1991). Recent studies have indicated that in alveolar proteinosis in which an abnormal form of SP-A is produced (Hattori *et al.*, 1996) and in SP-A gene ablation or knockout mice (Korfhagen *et al.*, 1996), tubular myelin is absent in surfactant. SP-B is a highly conserved, hydrophobic 17-kDa dimer which can fuse lipid bilayer membranes containing acidic lipids (Baatz *et al.*, 1991; Poulain *et al.*, 1996). In contrast, SP-A is a water-soluble 650-kDa, octadecameric glycoprotein that causes extensive aggregation of DPPC liposomal vesicles (Casals *et al.*, 1993; Poulain *et al.*, 1992). It is presumed that, under physiological conditions, tubular myelin is formed by synergistic interactions between these lipids and proteins, although the precise interactions required for such associations are not clear to date (Williams, 1991; Poulain *et al.*, 1992; Possmayer, 1997). Despite various imaging and labeling efforts the exact localization of specific lipids and proteins in TM has never been clearly defined.

Atomic force microscopy (AFM) has become a powerful tool for imaging biological structures, embedded cellular organelles, and individual biological molecules (Lal and John, 1994; Hansma *et al.*, 1997). The advantage of AFM over conventional techniques, such as electron microscopy (EM), is that three-dimensional information regarding the materials can be obtained at the molecular level, without the heavy metal staining as in transmission EM or surface coating employed in scanning EM (Hansma *et al.*, 1997). The structures of unstained cellular organelles in thin sections embedded in typical polymeric materials used for EM histology, such as Lowicryl and London Resin-White (LR-White), have been characterized (Braet *et al.*, 1997; Yamamoto and Tashiro, 1994). In such sections, the organelles protrude out of the plane of the polymer surface, allowing the topography of such structures to be conveniently observed by AFM (Yamamoto and Tashiro, 1994). Some of the surface topographical features may be enhanced and rendered more easily detectable for AFM work by using gold-labeled antibodies directed toward some of the surface epitopes (Putman *et al.*, 1993; Yamashina and Shigeno, 1995). However, compared to EM, a major disadvantage of using AFM to image heterogeneously distributed structures and micro-organelles present in low abundance in cellular systems is that unambiguous identification of imaged structure is not always possible (Lal and Proksch, 1997). Many AFM studies conducted previously on cells could not accurately detect and discern organelles, which could easily be observed using preferential staining in electron microscopy (Yamshino and Shigeno, 1995; Lal and John, 1994). Also, AFM in air requires the sample to be embedded and laid in a planar fixed surface. Multimodal imaging using AFM, EM, and other techniques holds promise for generating more complete two- and three-dimensional structural studies of biomaterials (Lal and Porksch, 1997). We have studied some unique three-dimensional tubular structures found in low abundance in pulmonary surfactant using AFM in air on embedded thin sections used for EM. The distribution and topography of gold-labeled antibodies to surfactant protein A on such tubular structures were also examined. The study suggests a simple approach for the unambiguous localization and imaging of lipid–protein structures with AFM and potential methods for identifying proteins in such systems.

MATERIALS AND METHODS

Isolation of bovine pulmonary surfactant. Pulmonary surfactant was isolated by lavaging freshly slaughtered bovine lungs with physiological saline by modification of methods discussed elsewhere (Yu *et al.*, 1983). Briefly, the lungs were lavaged with saline (0.15 M NaCl, 5 mM $CaCl_2$), and the resulting foamy suspension was frozen at −20°C. The suspension was briefly thawed and mixed with an equal volume of saline and centrifuged for an hour at 100*g*. The resultant white pellet was homogenized in saline and overlaid on 0.7 M sucrose in 0.1 M saline. The homogenate was diluted with equal volumes of saline and centrifuged at 50 000*g* (Sorvall, SS-34) for 1 h. The resultant surfactant layer was dispersed in saline and recentrifuged at 60 000*g* for 15 min, to a pellet. These processes allow for surfactant to contain all its lipid and associated proteins, and the product is termed bovine natural surfactant (Yu *et al.*, 1983).

Transmission electron microscopic (TEM) sample preparations. The bovine surfactant was reconstituted by incubating the suspension with occasional vortexing in buffer (5 mM Tris–HCl, 0.15 M NaCl, 5 mM $CaCl_2$, pH 7) at 37°C for 2 h. Samples were fixed in this buffer with 4% glutaraldehyde for 1 h at room temperature. Without further fixation, the samples were pelleted by centrifugation, transferred to flowthrough capsules, and processed for electron microscopy using an AFS device (Leica, Toronto, Ontario). Samples were embedded in either London Resin-White (Polyscience, Warrington, PA) or Lowicryl K4M (Chemische Werke Lowi, Waldkraiburg, Germany).

Samples processed into Lowicryl K4M were dehydrated in ethanol by progressive lowering of the temperature to −35°C, infiltrated in resin, and UV polymerized progressively at −35°C for 24 h, −4°C for 24 h, and 22°C for 24 h. Samples processed into LR-White were dehydrated similarly in acetone by progressive lowering of the temperature to −20°C. This was followed by a rinse in 100% ethanol to remove acetone, which is not compatible with LR-White. Embedding in LR-White was done in two steps, first 50% resin in alcohol at −20°C for 18 h and then 100% resin at

22°C, and the samples were polymerized at 60°C for 18 h (Hearn and Possmayer, 1997).

Ultrathin (70–100 nm) sections for both AFM and EM were made using glass and diamond knives. Sections for EM of 70 nm thickness in Lowicryl were collected on Butvar-coated nickel grids and stained using 1.5% uranyl acetate in 0.1% methyl cellulose, at pH 5.5, using previous methods of others (Roth *et al.*, 1990). Serial sections of the same Lowicryl-embedded samples used for EM were collected on chromosulfuric washed glass slides and used for AFM (without staining). Similarly, sections of LR-White (~95 nm) were collected on uncoated nickel grids for EM and on glass for AFM. The EM sections were stained with 3% uranyl acetate in 30% ethanol. Postembedding immunogold labeling for SP-A used a rabbit anti-SP-A antibody (generously provided by J. Whitsett, Division of Pulmonary Biology, University of Cincinnati) and a secondary antibody conjugated to 5 nm colloidal gold particles. Negative controls omitted the primary antibody or used an irrelevant antibody such as rabbit anti-catalase. Transmission electron microscopy of the sections was performed on a Phillips 410 microscope at various magnifications; generally micrographs were taken at 17 000×.

Localization of tubular myelin in EM sections for AFM. Tubular myelin was located in the stained sections using EM and photographed. The exact locations of the patches containing maximal amount of TM were marked in the photographs, and their distances from each edge of the rectangular sections measured in micrometers. The unstained parallel sections, deposited on glass, were observed under the optical zoom camera (used for localizing the tip alignments for AFM) of an atomic force microscope (Nanoscope IIIa; Digital Instruments, Santa Barbara, CA). The patches containing TM found using EM micrographs were selected for detailed study using AFM. These regions were scanned initially at low magnification using tapping and contact mode in AFM (100 × 100 μm).

Atomic force microscopy. Atomic force microscopy of the regions detected to contain TM in the Lowicryl and LR-White sections was performed in air using contact and tapping modes, using either a 120-μm (J) or a 12-μm (E) scanner. The sections placed on glass were fixed to a magnetic aluminum disk and mounted on the piezoelectric scanner for imaging. Commercial gold-coated silicon nitride 200-μm triangular cantilevers or Nanoprobe SPM tips (Wafer 113-135-22; Digital Instruments), with nominal spring constants of 0.06 or 0.38 N/m were used for contact and lateral force (friction) imaging. Tapping-mode images were obtained using 125-μm silicon nitride beam cantilevers or Nanosensors Point Probes (Wetzkar-Blankenfeld, Germany). Platinum tips of nominal radius of 20 nm were used for initial tapping-mode scans in the J scanner. After localization of TM in high-magnification scans, sharper tips of nominal radius below 10 nm and height 10 μm (Wafer Unit-11619L098, Digital Instruments) were used and the modes of scanning alternated between tapping and contact modes, using the E scanner. Typical scan rates of 0.25–0.5 Hz were used for 100- to 10 μm scans and 1 Hz for the 500- to 100 nm scans.

RESULTS

Figure 1a shows typical images of thin Lowicryl sections of embedded bovine pulmonary surfactant. A whole section, as seen under the optical camera of the AFM (A), as well as by electron microscopy (B), is shown, along with the zoomed-in area containing TM as observed by optical camera (C) and atomic force (D) microscopy. The AFM micrograph (D) shows that the surfaces of the sections have patterns similar to those seen by the optical method (C). The black and white patch in (C) was osmium tetraoxide stained and identified (B) by TEM to contain a large amount of tubular myelin. Figure 1b shows tapping-mode AFM micrographs with progressive increase in scan magnification (i–iii) of the region in Fig. 1a, D, the corresponding line section analysis of the surface (plots on the right), and an electron micrograph of this region (iv). At low magnification (100 μm; i), the surface of the sections shows even corrugations of about 90 nm (flat depression lines in the line sections) and other protrusions exceeding 200 nm. The 90-nm depressions suggest that the sections probably had holes (black regions), and the AFM tip penetrated the depth of these holes probably revealing the thickness of the section. Scanning beyond the edge of the section indicated that the tip dropoff from the section to the glass support was around 95 nm, a value close to the thickness of the sections. With 20 μm scans (Fig. 1b, ii) within the patch, the corrugations became more frequent, and with 2 μm scans (Fig. 1b, iii), the lattice network of TM became clearly visible. The TM structures were seen as 5- to 10-nm surface bumps (Fig. 1b, iii), and the regions containing such structures were found to be elevated by about 50 nm above the rest of the section.

From Fig. 2A it is evident that the tubular bumps or ends are about 2 nm in height and are spaced about 50 nm apart, as can be seen in the line section analysis. The three-dimensional image of the surface in Fig. 2B also attests to the fact that regions of TM are located in elevated and depressed regions of the Lowicryl sections. Higher magnification (C) of a selected region of image shown in (B) showed the lattice network, as seen in the electron micrograph from this region (D). The EM image in (D) indicated that the TM stains with almost perfectly square lattices and that such regions have some peculiar cross-hatch patterns, which are not clearly visible in the high magnification AFM image in (C). Previous studies have suggested that these cross-hatch structures may be surfactant protein A embedded in the lipid-tubular core (Beckmann and Dierichs, 1984). The surface textures of TM in the Lowicryl sections seen here are in agreement with previous studies by scanning electron microscopy of bacterial sections in which specimen-related reliefs of 5–6 nm were found near membranous organelles (Kellenberger *et al.*, 1987). Some of the surface texture of the larger areas of the section observed by AFM at low magnification corresponds to previously published images of sections of cellular regions embedded in different polymeric resins observed using AFM (Yamamoto and Tashiro, 1994; Braet *et al.*, 1997). Previous TEM studies of stained sections of tubular myelin have revealed that some regions of the square lattice networks are more visible than others in the micro-

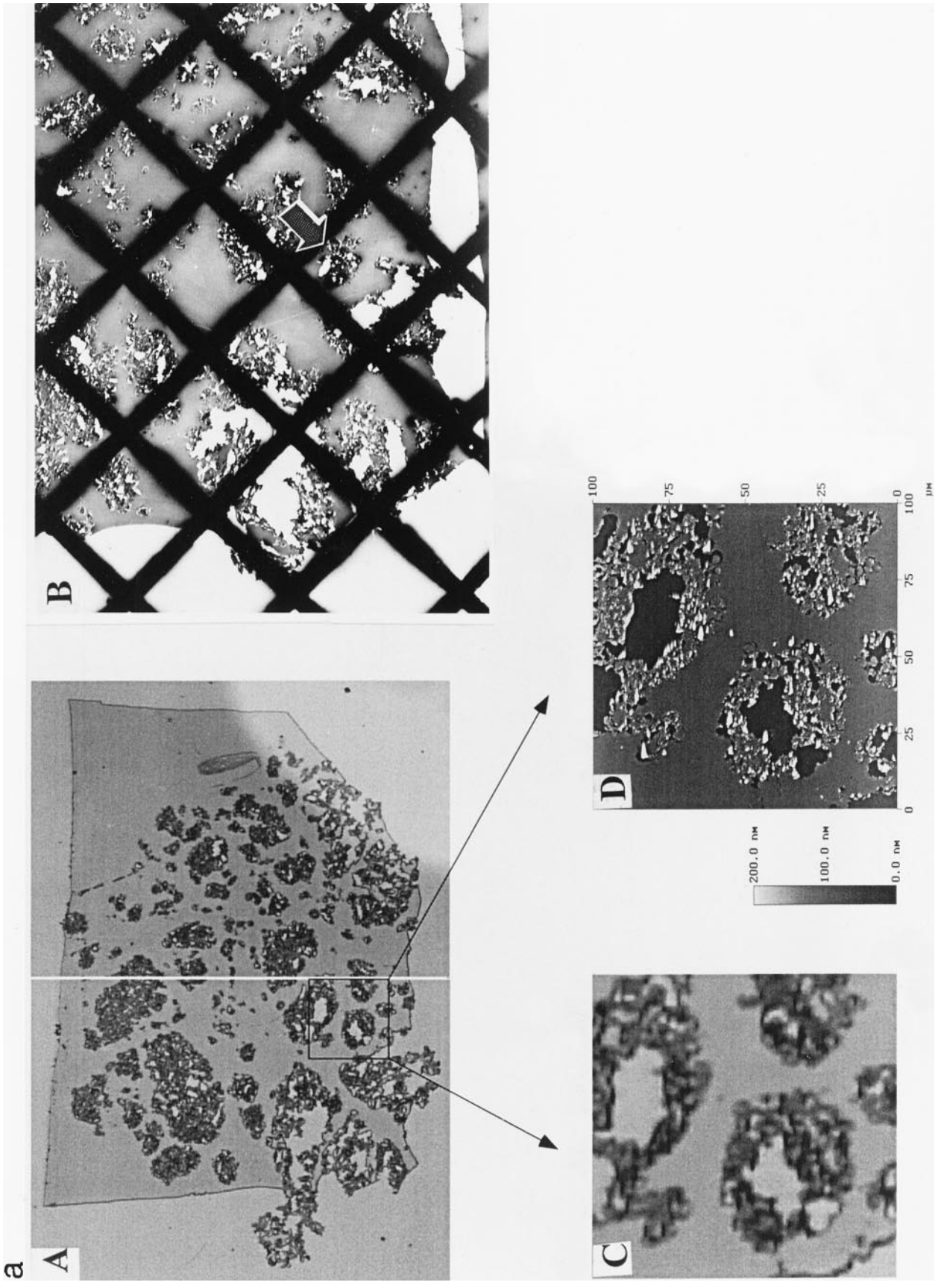

FIG. 1. Typical images of Lowicryl-embedded sections of pulmonary surfactant containing tubular myelin using transmission electron and atomic force microscopy in air. (a) The localization of the regions containing TM were performed by mapping the regions in the complete section seen by optical method (A) and using transmission electron (B), optical (C), and atomic force microscopy (D) in tapping mode. The area containing TM is shown by the arrow in the electron micrograph in (B). (b) The progressive higher magnification scans of this region using AFM (i–iii) and an EM of the region (iv) are shown. The right-hand plots of (i–iii) represent the line scan data plotted as a function of distance of the lines indicated in the images. The bars to the right of the images in (b) represent the vertical height profiles representative of the gray-scale values in each image (black—lowest, white—highest).

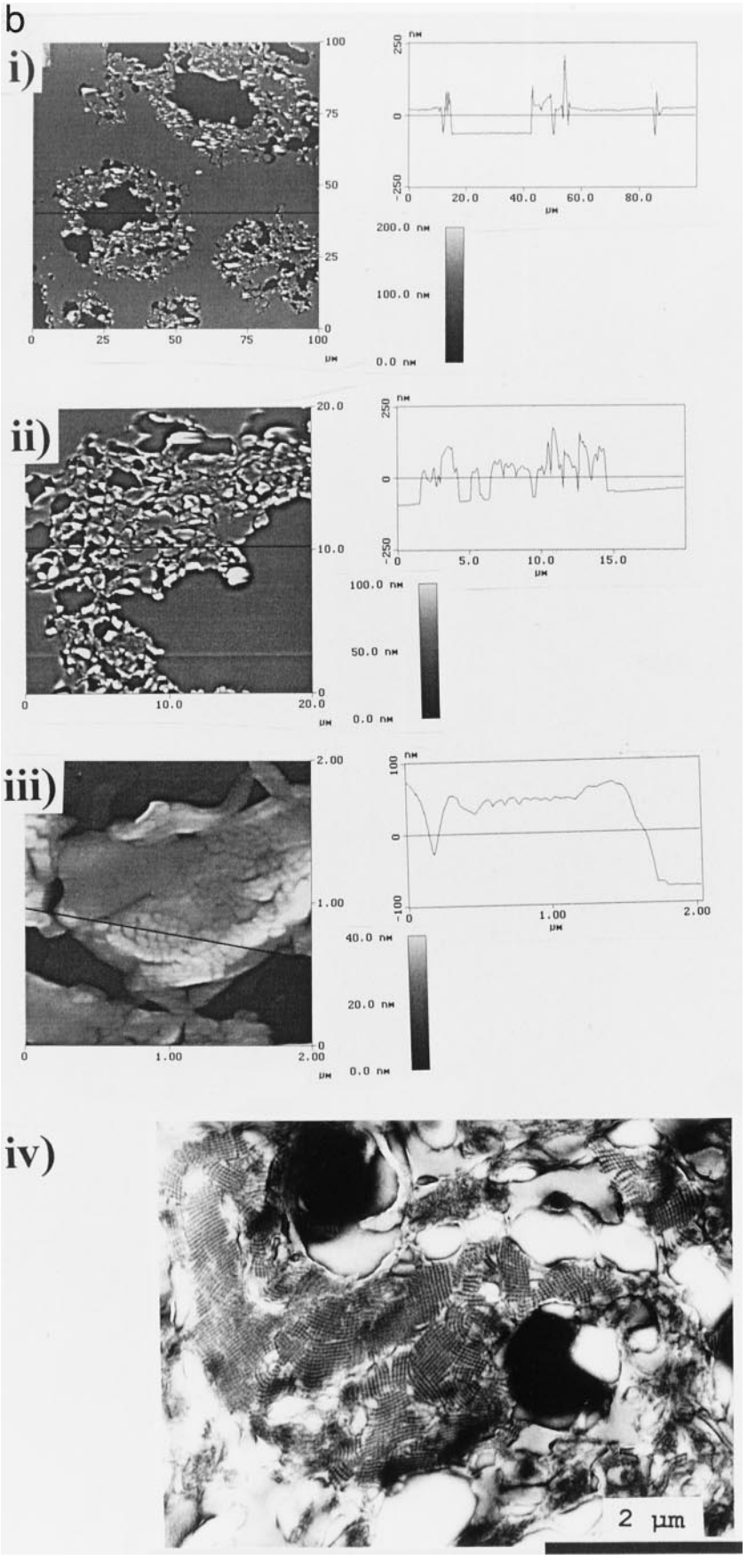

Fig. 1—*Continued*

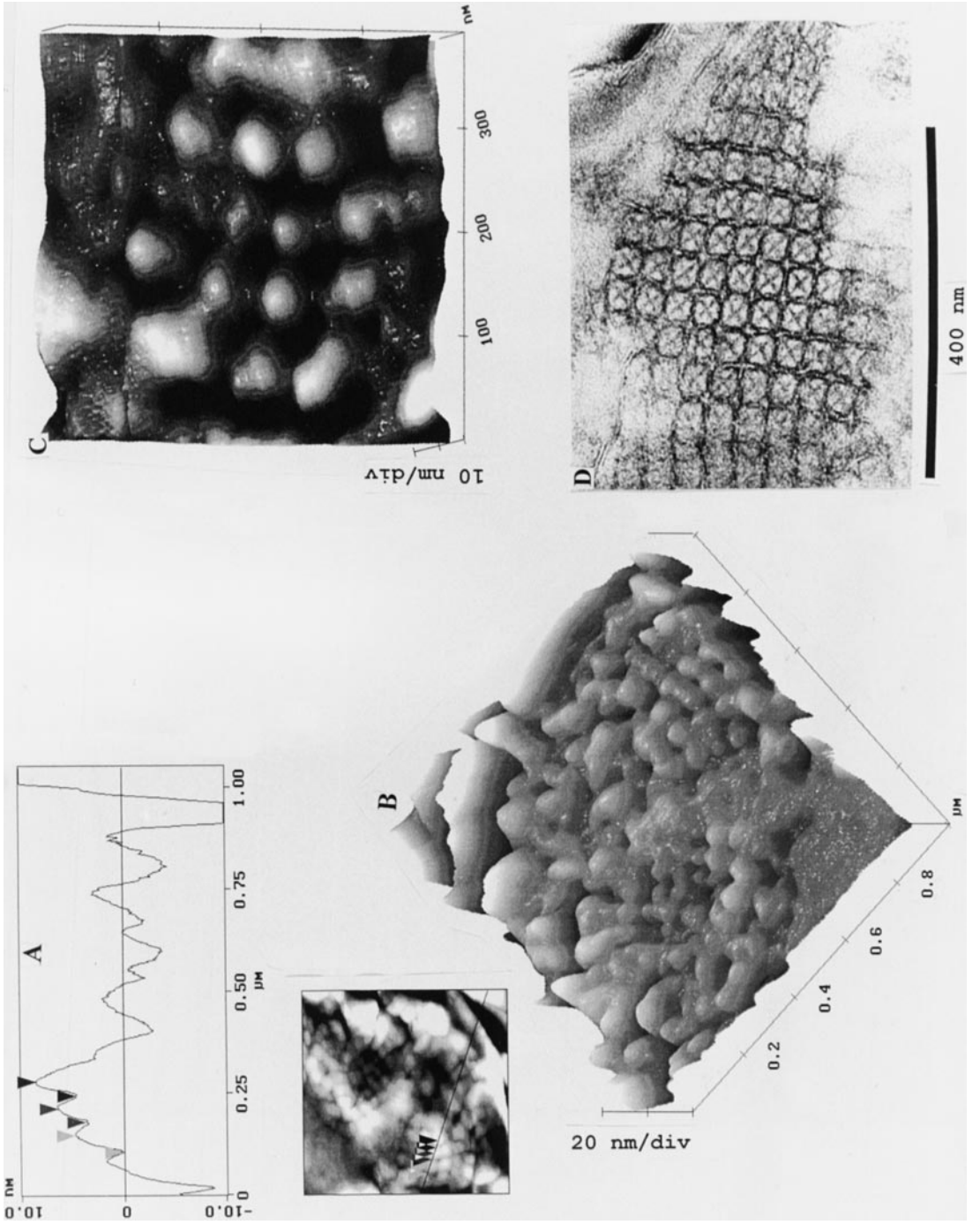

FIG. 2. The two-dimensional line scan and image (A) and three-dimensional images (B and C) of tubular myelin observed in tapping-mode AFM and the electron micrograph taken from the same region (D) at high magnification. The images in (B) indicate that tubular myelin is located in uneven surfaces of Lowicryl, and such surface contours probably diminish the contrast of the tubes in some parts of the EM image (D). The line section (A) indicates that the open ends of the tubes are 40- to 50-nm laterally spaced bumps of ~5 nm vertical height, located along a slanted surface to the plane of the section. The EM image (D) also indicates cross-hatched structures in the center of the tubes (probably protein) and shows that some internal structures of the tubes can be stained.

graphs (Gil and Reiss, 1978). It is possible that these regions were not clearly visible in the earlier TEM studies due to such regions lying in the 5- to 10 nm depressions from the plane of the surface of sections, whereas the visible parts are in the elevated regions, as shown in Fig. 2B.

The typical dimensions, obtained by EM and AFM of tubular myelin are shown in the plots in Fig. 3A. The areas for the lattices in the AFM images were calculated by considering the typical radius of the circular regions. The distances in both images were calculated by determining the approximate center of the squares (in EM) and circle or ellipse (in AFM, as in Fig. 2) and measuring the nearest neighbor distance between any two tubes for an average of 20 tubes. As observed the distance between the centers of tubes in the TEM (Fig. 3A, left) is between 30 and 45 nm, whereas for the AFM (Fig. 3A, right) it is between 35 and 75 nm. The increases in the average distances in the AFM images compared to those of TEM were probably due either to tip/sample interactions or to tip convolutions blurring the images or both. It is also conceivable that the differences arising between EM and AFM morphometry are due to either the AFM images indicating the three-dimensional nature of the tubes, resulting in their lying at different planes of the sample or our not being able to accurately determine the exact centers of the circular or elliptical cross section of the tubes, or both. The former explanation seems feasible in the context of a previous study, in which 30 nm (by EM) gold particles were observed by AFM as being about 80 nm due to tip/sample convolutions (Putman *et al.*, 1993). However, the areas occupied by the tubes are similar, in TEM and AFM images, indicating that the internal areas of the tubes can be measured consistently using either technique, although resolution by each technique shows differences in the shapes of the structures. The dimensions of the tubes using AFM and TEM are in approximate agreement with each other and with those (published previously) in native and reconstituted TM by EM (Weibel and Gil, 1968; Williams, 1979; Suzuki *et al.*, 1989).

Other structures present in the tubular myelin lattice observed at higher resolutions are shown in Figs. 3B and 3C. Previous studies have suggested that TM is formed by fusion of open bilayer lamella of secretory vesicular structures of pulmonary surfactant or lamellar bodies (LB) (Williams, 1979; Froh *et al.*, 1990; Young *et al.*, 1992). Others using dye penetration of sections containing TM with attached multiple lamellar bodies have suggested that several lamella of the LB simultaneously contribute material to the tubes (Young *et al.*, 1992). In TEM, as shown in Fig. 3B, right, the tubular myelin-rich areas were observed to have lamellate or bilayer-containing areas in their periphery (arrow). A typical AFM image (Fig. 3B, left) of these regions indicates that the lamella can be observed as broad black streaks or canal-like regions, with some parts elevated. These elevated regions (white in B, left) have heights of 2–5 nm, which correspond to the typical height of the tubular myelin protrusions as seen in Fig. 2. This may indicate that the white areas represent regions where the bilayers fuse and form the square tubes.

To observe whether the cross-hatch features could be observed by AFM (as shown in Fig. 2D) higher magnification scans were performed on the tubes using sharper tips (nominal radius below 10 nm) and are shown in Fig. 3C. The two-dimensional (left) and three-dimensional (right) AFM images in (Fig. 3C) were scanned at 100 nm and indicated that some of the tubes have multilobes which can be seen readily at such resolution. Even using the sharper tips, no further features could be observed, and there were some tip–sample interactions which frequently gave regions which looked flushed out (arrows in Fig. 3C). The cross hatches as shown in the TEM image in Fig. 2 (and possibly in the bilobe structures seen in AFM) were previously suggested by others to be surfactant protein (probably SP-A) associated with the lipid membranes of TM (Beckman and Dierichs, 1984; Voorhout *et al.*, 1991), although freeze-fracture scanning EM has failed to reveal any internal structures in the core of the tubes (Chi and Lagunoff, 1978; VanGolde *et al.*, 1994).

Previous studies using AFM have revealed that tip/sample convolutions can indicate different shapes and sizes of objects in AFM compared to their molecularly correct dimensions and that these problems can sometimes be remedied by using various scanning modes of the same sample (Putman *et al.*, 1993; Santos *et al.*, 1998). Most of the AFM images suggested that the cores of the TM tubes were semicircular bumps or regions in the 3D or 2D images, respectively, whereas the TEM images indicated the structures were squares or rectangles. In tapping mode AFM, the topography of the lattices was found to be somewhat more rectangular, at least in phase images as shown in Fig. 4A, right. In the contact-mode AFM, the hemispherical bumps of TM were also found to be similar to those in the tapping-mode images when the height topography (with *z* axis) was displayed (Fig. 4B, left). The same AFM images displayed in friction mode indicated the lattices were square, as shown in Fig. 4B, right. Line section (Fig. 4C) and 3D friction topography (Fig. 4D) of this region indicated that the AFM tip experienced greater frictional forces at the corners and edges of the TM, thereby providing greater similarity to the square-lattice structures seen in TEM. The line

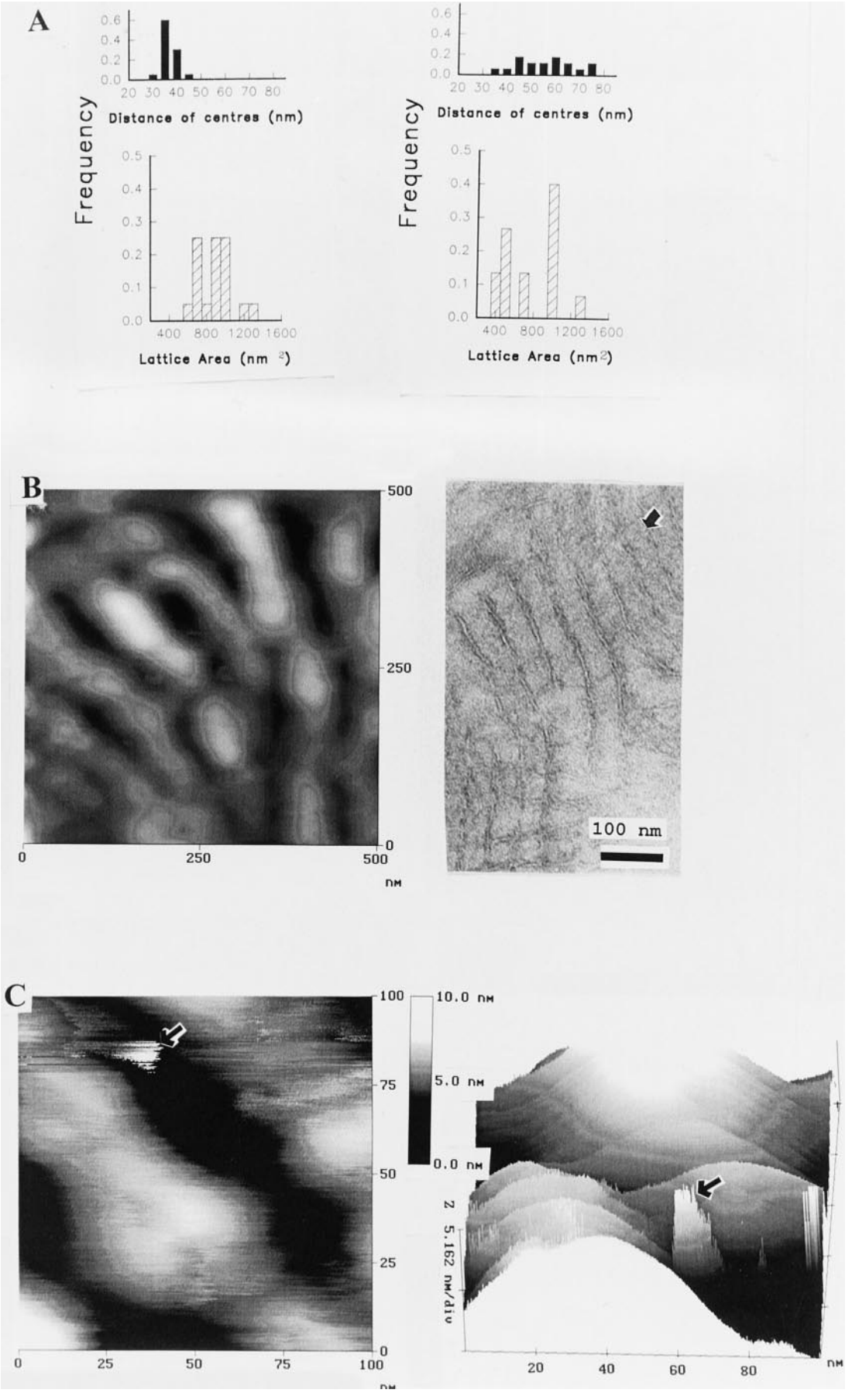
A
Frequency
Distance of centres (nm)
Lattice Area (nm ²)
Frequency
Distance of centres (nm)
Lattice Area (nm²)
B
100 nm
nm
C
10.0 nm
5.0 nm
0.0 nm
Z 5.162 nm/div
nm

section analysis shown in Fig. 4C indicated that the frictional forces at the corners of the TM generated better or sharper features of the Lowicryl surface, compared to those visualized using height mode imaging. The square structures of TM obtained here by contact-mode AFM closely resemble those seen previously in freeze-fracture replicas of TM by others using scanning EM (Williams, 1978; Manabe, 1979; Van Golde *et al.*, 1994).

Previous studies have indicated that the lipidic bilayer matrices of TM can be removed by acetone washing, leaving the interior skeletons of the tubes intact (Beckmann and Dierichs, 1984). This technique requires the use of embedding materials other than Lowicryl, which can copolymerize with the protein materials of the tubes (Beckmann and Dierichs, 1984). Typical TEM images of acetone-washed tubular myelin embedded in LR-White are shown in Fig. 5B, and that for nonextracted TM in Lowicryl with the bilayers intact is shown in Fig. 5A for comparison. The LR-White section (Fig. 5B) indicated that the shape of the tube lattices becomes rectangular rather than square, and removal of the lipid bilayer by washing results in an increase in the distance between adjacent lattice tubes. The cross-like structures observed inside the tubes in TEM also become more prominent compared to native TM sections in Lowicryl (Fig. 5A). AFM surface topography of all acetone-washed LR-White sections of TM (for example, a region of Fig. 5B) indicated that the surfaces were very smooth, and no features were discernable with scans of 100 μm to 500 nm (data not shown). However, in contact-mode AFM, these LR-White sections containing TM skeletons became vaguely visible at high magnification in 3D, as shown in the bottom of Fig. 5C. A magnified TEM view of the rectangular regions of LR-White sections is shown above the AFM topography. The cross rectangles correspond somewhat to the black undefined shaped holes in the AFM images (bottom). Also as seen in the AFM image, the surface of the LR-White had heterogeneous height profiles of corrugated surfaces of 2–5 nm, which could possibly be the polymer matrix of the resin. The most interesting AFM feature of the LR-White-embedded TM was that the rectangular tube surfaces resembled depressions instead of the hemispherical bumps or protrusions observed in all Lowicryl sections (Figs. 1–4). This could be due either to the property of the LR-White resin compared to Lowicryl or to the property of the TM tubes after the lipid bilayers have been removed. It is also reasonable to conclude that the cross-hatches in the TEM sections of TM skeletons are highly stainable but have little 3D topography, as seen in AFM. Previous AFM studies of LR-White sections of cellular organelles have indicated similar smooth surfaces for this resin (Yamamoto and Tashiro, 1994). The AFM images published by these authors also indicated 6 nm depressions for the plasma membranous regions of the cellular organelles containing membrane proteins, which suggest that LR-White embedding may not penetrate proteinaceous regions (Yamamoto and Tashiro, 1994), as also seen in this study.

In an attempt to localize SP-A in the LR-White sections shown above, the regions containing TM skeletons were labeled with gold particles (diameter of 5 nm) conjugated to antibodies to the protein. Typical TEM images (Fig. 6A) and corresponding AFM images (Fig. 6B) of such regions are shown. The black dots in the TEM image represent the 5-nm gold particles (Fig. 6A), which are observed as sharp bumps in AFM (Fig. 6B). Similar protrusions of gold particles in antibodies have been observed by others using AFM (Putman *et al.*, 1993). Both the images indicated that the gold particles were localized heavily, but somewhat randomly in the regions containing the "protein" skeletal lattice of the TM. These images indicate that the protein is localized within the square-lattice regions, although it was not possible to discern the X-shaped structures as seen with staining in the EM (Fig. 6A). The random distribution of the gold labels may be due to the gold particle located farther away from the proteins, due to its random localization in the surface of the antibody, or perhaps no epitope was available to the fixing and embedding process. Whatever the case, the gold antibody labeling techniques could not be used to conclusively localize surfactant proteins in TM, in either stained or unstained sections. Previous studies have suggested that such labeling techniques can yield the localization of the proteins within 20 nm of the lattice corners of the TM (Voorhout *et al.*, 1991).

FIG. 3. (A) Comparative quantitative analysis of tubular myelin dimensions using TEM (left) and AFM (right) and (B and C) AFM of high-magnification structures associated with TM of Lowicryl sections. The dimension analysis was done on 20 lattices by measuring the distance and area dimensions of the square (by EM; A, left) or circular tubes (by AFM; A, right). (B) The lamellate structures associated with tubular myelin as observed by AFM (left) and EM (right). The thickness of the lamella (arrow in B) as observed by EM agrees with those of typical phospholipid bilayer membranes. (C) A 2D high-magnification scan of tubular myelin cores obtained using tapping mode AFM. The 3D image of the scan is shown at the right. Tip sample interactions frequently lead to the appearance of certain flushed out regions (arrows in C) in the high-magnification scans.

DISCUSSION

Tubular myelin accounts for a small percentage of pulmonary surfactant structures. Limited three-dimensional information of such structures is avail-

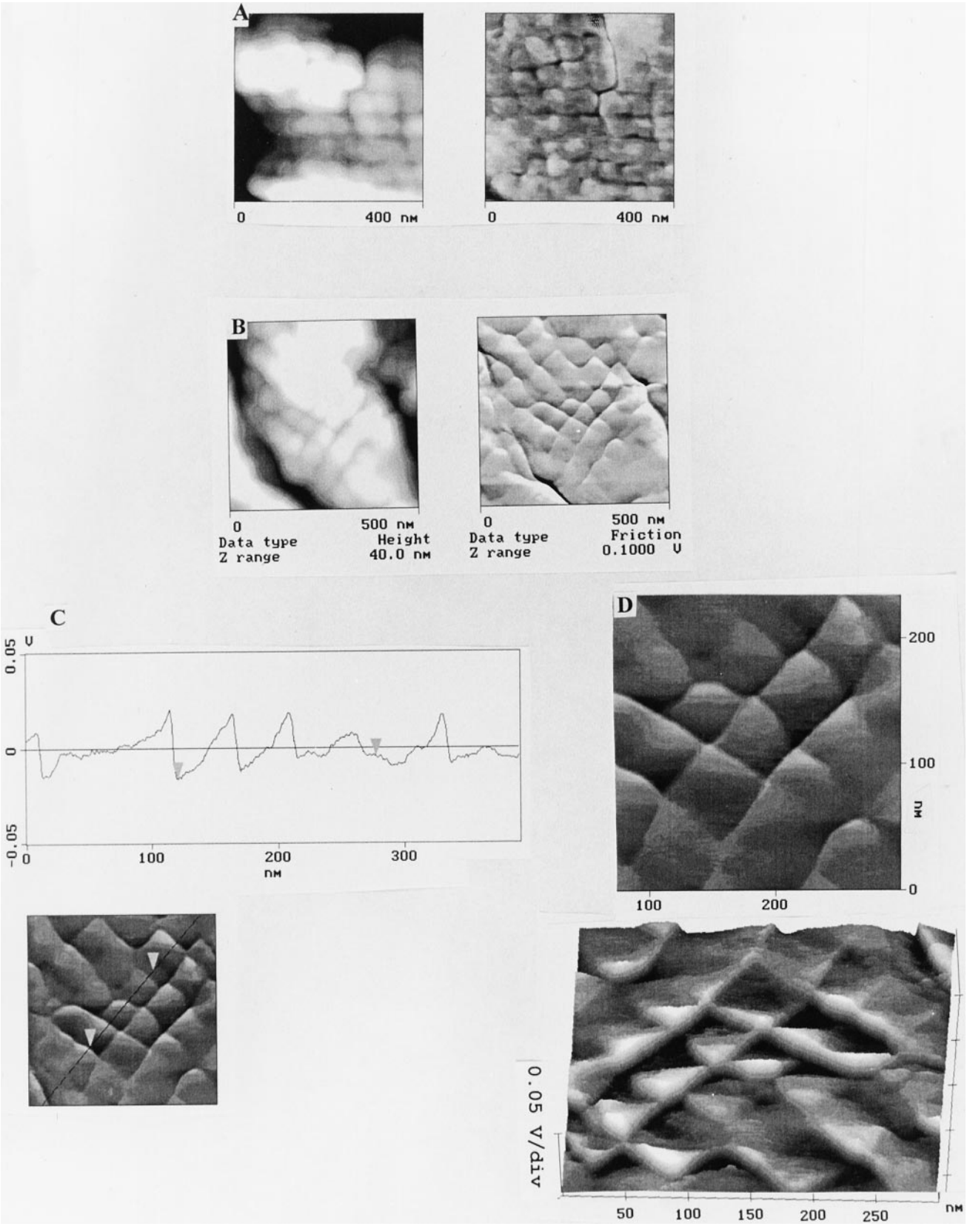

FIG. 4. Typical AFM images of tubular myelin (unstained) obtained using (A) phase and (B–D) friction-mode imaging, revealing the square-lattice arrangement of the tubes as typically observed by electron microscopy of the stained material. The corresponding height-mode images are shown on the left of (A) and (B). The line section analysis of the friction-mode image (C) and its 3D representation (D) are shown. The edges and corners of the tubes had sharp frictional or higher torsional interactions with the AFM tip (D, bottom), and the EM stains possibly can be localized in such sharp vertical corrugations.

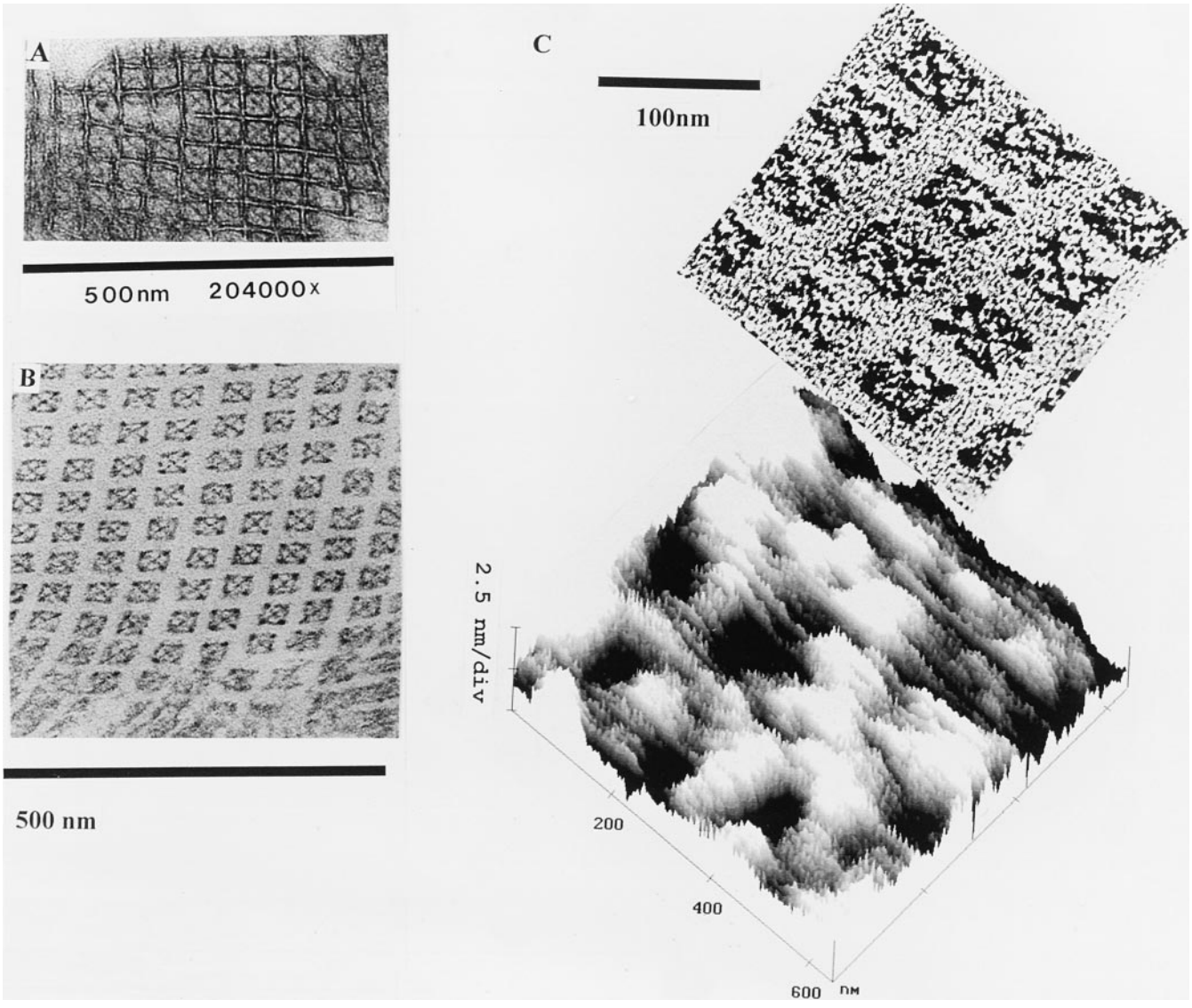

FIG. 5. Typical EM micrographs of tubular myelin sections before (A) and after (B) acetone washing to remove the lipid bilayers, and a comparative AFM of a region from (B) is shown in (C). The top image in (C) is an enlarged electron micrograph of the images in (B) for comparison with the AFM (bottom) at a similar magnification. Sections in which the lipids were removed by acetone washing (B and C) were embedded in LR-White and possibly consist of the protein cores of the tubes. The AFM image (C, bottom) indicated these regions to be hollow (black) compared to the smooth background of LR-White (white corrugated regions). The localization of the depressions (black) in the AFM image (C, bottom) somewhat correlates to the crossed rectangles in the top image but only for a few lattices.

able using scanning electron microscopy (Chi and Lagunoff, 1978; Williams, 1978; Manabe, 1979) and reconstructions based on computer modeling (Young *et al.*, 1992). Part of the difficulty in obtaining information on TM is due to its relatively low abundance found in the natural surfactant or in reconstituted systems (5–10%) (Benson *et al.*, 1984; Hawgood, 1997). A multimodal approach using techniques such as electron and atomic force microscopy on the same macromolecular complex may yield specific three-dimensional information on such systems (Lal and Proksch, 1997). Recent studies using AFM on electron microscopy sections of whole cells have shown that additional information on organelle structures which was not available using either technique by itself, can be obtained (Braet *et al.*, 1997; Canet *et al.*, 1996). The limitations of applying AFM imaging to mixed complex macromolecular systems lie in the somewhat arbitrary identification of the imaged structures, since the three-dimensional surface topography of biological structures may be different from the two-dimensional images obtained using techniques such as transmission electron microscopy. This problem is further en-

hanced when using techniques such as atomic force microscopy in air to study TM, in which unambiguous localization of materials is of critical importance (Lal and Proksch, 1997). Since TEM techniques use stained electron-dense materials which are easy to localize at low magnification, combining TEM with AFM allows for precise localization of such macromolecular complexes, as specifically demonstrated in this study (Fig. 1).

Cellular organelles from various tissues embedded in various EM polymeric matrices have been examined using AFM in air of thin sections on planar surfaces (Amako *et al.*, 1993; Braet *et al.*, 1997; Canet *et al.*, 1996; Ushiki *et al.*, 1994, 1996; Yamamoto and Tashiro, 1994). Although some of these studies revealed the three-dimensional structures of the whole cell, unambiguous identification of intracellular organelles was not possible. The typical surfaces of the sections of pulmonary surfactant embedded in Lowicryl indicated multifaceted corrugation or surface roughness ranging from 2 up to 90 nm. Tubular myelin was easily located in such Lowicryl sections as 2- to 5-nm protrusions, suggesting some similarities with previous attempts to localize cellular organelles using AFM (Yammoto and Tashiro, 1994). Some studies have suggested that biological tissue sections used for TEM possess different degrees of surface roughness, depending on the polymeric materials used (Yamamoto and Tashiro, 1994). Others have shown that due to the lack of copolymerization of some biological materials with embedding materials, such as Lowicryl, the cleavage (or sectioning) surface follows areas of least resistance and epitopes are laid open in such surface sections (Kellenberger *et al.*, 1987). The path of least resistance during cutting or sectioning of polymer-embedded cell organelles is provided normally by the interfaces between the polymeric resins and proteins (Kellenberger *et al.*, 1987). The reason this process occurs during cutting is that the tissues are embedded at low temperature and cleaved at higher ambient temperature. It has been suggested that since progressive subzero lowering of temperatures is usually used to embed such sections, the hydration shells of the proteins may possibly be lost at room temperatures, thereby causing specimen-related reliefs or depressions in the surface plane of the sections (Carleman *et al.*, 1985). Although such surface reliefs are not visible using TEM, a surface topographical method such as atomic force microscopy can be employed to observe such three-dimensional heterogeneity on section surfaces, thus possibly allowing one to map the open-ended tubular protrusions of the TM. The topographical bumps as seen in the Lowicryl sections of TM could be proteins such as SP-A protruding out of the embedded lipid tubular cores.

Embedding TM in Lowicryl or polymer matrix had a specific advantage for AFM, since previous studies have indicated that soft biological materials can undergo deformations under the AFM tip due to nano-Newton forces applied on the samples (Hansma *et al.*, 1997). The polymer matrix permits features to be observed, but tip–sample interactions can cause the TM structures to be observed as circular rather than square regions, as in the tapping-mode images of Figs. 1–3. We expect that the convolutions due to tip–sample interactions will lead to larger lateral dimensions of the small structures, but it has been shown that the AFM will reflect the correct vertical heights (Putman *et al.*, 1993). As observed in some of the images at high-magnification scan (Fig. 3C), the internal structures of the tubes could not be clearly observed using AFM, since it is possible that the width-to-height aspect ratio of the tip may not have allowed for tip penetration in finer grooves of TM. A note of caution should be mentioned here in interpreting the results, since the penetration properties of the embedding materials in different lipid- and protein-rich regions is not known at present. However, small regions where the lattice networks were seen in AFM (Fig. 2C) could be interpreted as areas of the sections where such ambiguities were minimized with the best embedment. Some of the surface epitopes observed in the study of TM (Figs. 2–5) may be dependent on property of penetration of the matrix in to the lipid–protein tubes and may thereby lead to ambiguities and the change of the state of preservation of the samples. However, in contact mode (Fig. 4), the square lattices were clearly observed and the edges of the tubes had higher frictions than their centers. These images of TM (Figs. 4B and 4C) were very similar to the ones obtained previously by others using freeze-fracture scanning electron microscopy (Van Golde *et al.*, 1994; Williams, 1978; Manabe, 1979).

It is difficult to determine whether the change of the shape of the square lattices to rectangular in the LR-White sections (Fig. 5) is due to removal of the lipids or to the property of the resin. Attempts to remove the lipids from TM in Lowicryl-embedded sections were not successful due to possible interactions of Lowicryl with acetone, and thus comparative studies of TM between such resins were not possible. Also, at low magnification the surface of the LR-White was found to be smoother compared to Lowicryl, and therefore unambiguous localization of TM was difficult using either contact or tapping mode. Previous studies using AFM have also indicated similar levels of surface heterogeneity in different resins including those used here (Amako *et al.*, 1993;

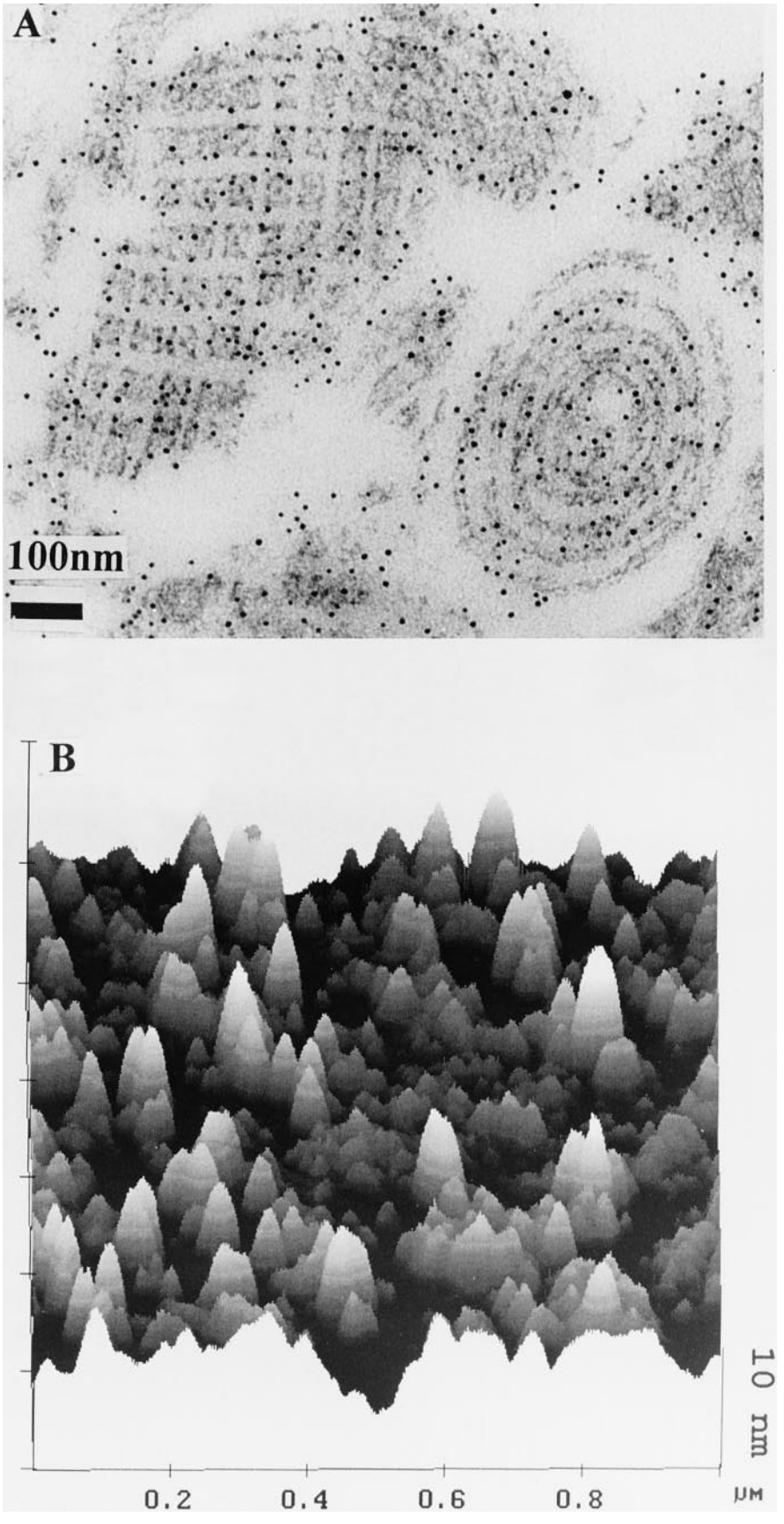

FIG. 6. Typical EM (A) and AFM (B) images of the LR-White sections (as in Fig. 5) surface labeled with 5 nm gold particle-conjugated anti-SP-A antibody. The gold particles are seen as sharp 5- to 10 nm bumps (white peaks, B) in AFM and are distributed heavily in the regions containing the TM as seen by either technique.

Yamamoto and Tashiro, 1994), and therefore the smoother resins should be avoided for AFM work. Recently others have reported techniques in which limited amount of the resin can be removed from such sections, thereby limiting the effect of the resin on the biological materials (Ushiki *et al.*, 1996, 1994). Such techniques would probably indicate better three-dimensional topography of tubular myelin using AFM, although the effects of embedding–deembedding on the epitopes are not known at present (Ushiki *et al.*, 1996).

The AFM features of TM in Lowicryl indicate that the centers of the tubes could contain proteinaceous materials, since others have indicated that the cleavage path of the sections follows the regions containing proteins (Kellenberger *et al.*, 1987). It has been suggested, based on antibody labeling, that SP-A is localized near the corners of tubular myelin (Voorhout *et al.*, 1991; VanGolde *et al.*, 1994), but this has not been observed by all investigators (Walker *et al.*, 1986; Hearn and Possmayer, 1997). Still other TEM studies have shown that small (8 nm) extramembranous particles, presumed to be surfactant proteins (SP-A), are attached to the lipid tubes (Beckman and Dierichs, 1984). It is difficult to obtain structural localization of proteins in TM using antibody labeling, because the large antibody may hide specific features of the antigen and the gold label on the antibody need not be localized exactly at the locale of the epitope but in its surrounding vicinity. We failed to localize SP-A precisely in the TM in our study (Fig. 6), even though the AFM images clearly indicated localization of the gold particles. Previous gold-labeled antibody studies using TEM have indicated that the antibody to SP-A could be located within a 20-nm vicinity of the corners of tubular myelin (Voorhout *et al.*, 1991). Generally TM labels heavily with the anti-SP-A antibody, but the gold labels are located somewhat randomly around such regions (Walker *et al.*, 1986; Hearn and Possmayer, 1997). The location of the lipid bilayers in the TM observed by AFM indicated that the bilayers were noted as 5- to 10 nm surface depressions in the Lowicryl sections. In previous studies of hepatocytes and kidney cells using AFM, the plasma membranes were observed as 6 nm depressions in surfaces of Lowicryl sections (Yamamoto and Toshiro, 1994).

In summary, we report here the three-dimensional structures of nanotubules (tubular myelin) found in relatively small abundance in lung surfactant using atomic force microscopy. We also suggest how such a nanoscale structure in a complex macromolecular lipid–protein system can be unambiguously identified in AFM in air. The surface of the tubes of TM could be observed as 40-nm-wide and 5- to 10-nm-deep protrusions or depressions using AFM, and such features reflect possible distribution of proteins in TM. The tubular myelin had dimensions and square-lattice distributions relatively similar to those observed by EM and AFM. No specific protein or internal structures of TM could be discerned either using antibody labeling or in direct surface topography mapping in AFM. The study suggests a relatively simple multimodal approach to detecting unambiguously specific biological structures by AFM and possible lipid–protein arrangements in three dimensions.

The authors acknowledge the technical assistance provided by Mr. John Graham (Department of Chemistry, University of Western Ontario) with the AFM. The work was supported in part by grants from the Medical Research Council (to F.P. and K.N.) and the National Scientific and Educational Research Council of Canada (to N.O.P. and J.G.M.). The study was also supported by a Canadian Lung Association/MRC joint postdoctoral fellowship (to K.N.) and a block term grant from the Ontario Thoracic Society (to K.N. and F.P.).

REFERENCES

Amako, K., Takeda, A., Umeda, A., and Yoshida, M. (1993) Imaging of the surface structures of Epon thin sections created with a glass knife and diamond knife by atomic force microscope, *J. Electron Microsc.* **42,** 121–123.

Baatz, J. E., Sarin, V., Absolom, D. R., Baxter, C., and Whitsett, J. A. (1991) Effects of surfactant associated protein SP-B synthetic analogs on the structure and surface activity of model membrane bilayers, *Chem. Phys. Lipids* **60,** 163–178.

Beckmann, H.-J., and Dierichs, R. (1984) Extramembranous particles and structural variations of tubular myelin figures in rat lung surfactant, *J. Ultrastruct. Res.* **86,** 57–66.

Benson, B. J., Williams, M. C., Sueishi, K., Goerke, J., and Sargeant, T. (1984) Role of calcium ions in the structure function of pulmonary surfactant, *Biochim. Biophys. Acta* **793,** 18–27.

Braet, F., Dezanger, R., and Wisse, E. (1997) Drying cells for SEM, AFM and TEM by hexamethyldisilazine—A study on hepatic endothelial cells, *J. Microsc.* **186,** 84–87.

Canet, D., Rohr, R., Chamel, A., and Guillain, F. (1996) Atomic force microscopy study of isolated ivy leaf cuticles observed directly after embedding in Epon, *New Phytol.* **134,** 571–577.

Carlemam, E., Villiger, W., Hobot, J. A., Acetrin, J. D., and Kellenberger, E. (1985) Low temperature embedding with Lowicryl resins: Two new formulations and some applications, *J. Microsc.* **140,** 55–63.

Casals, C., Miguel, E., and Perez-Gil, J. (1993) Tryptophan fluorescence study on the interaction of pulmonary surfactant protein A with phospholipid vesicles, *Biochem. J.* **296,** 585–593.

Chi, P. Y., and Lagunoff, D. L. (1978) Linear arrays of intramembranous particles in pulmonary tubular myelin, *Proc. Natl. Acad. Sci. USA* **75,** 6225–6229.

Dobbs, L. G., Plan, M. S., Maglio, M., Dumars, S., and Allen, L. (1997) Maintenance of the differentiated type II cell phenotype by culture with an apical air surface, *Am. J. Physiol.* **273,** 347–345.

Effrati, H., Hawgood, S., Williams, M. C., Hong, K., and Benson, B. (1987) Divalent cation and hydrogen ion effects on the structure and surface activity of pulmonary surfactant, *Biochemistry* **26,** 7986–7993.

Froh, D., Ballard, P. L., Williams, M. C., Gonzales, J., Goerke, J., Odom, M. W., and Gonzales, L. W. (1990) Lamellar bodies of cultures human fetal lung: Content of surfactant protein A (SP-A), surface film formation and structural transformation in vitro, *Biochim. Biophys. Acta* **1052,** 78–89.

Gil, J., and Reiss, O. K. (1973) Isolation and characterization of lamellar bodies and tubular myelin from rat lung homogenates, *J. Cell Biol.* **58,** 152–171.

Goerke, J., and Clements, J. A. (1986) Alveolar surface tension and lung surfactant. *In* Macklem, P. T., and Mead, J. (Eds.), Handbook of Physiology—The Respiratory System III, Mechanics of Breathing, pp. 247–261, Am. Physiol. Soc., Washington, DC.

Hansma, H. G., Kim, K. J., Laney, D. E., Garcia, R. A., Argaman, M., Allen, M. J., and Parson, S. M. (1997) Properties of biomolecules measured from atomic force microscope images: A review, *J. Struct. Biol.* **119,** 99–108.

Hattori, A., Kuroki, Y., Kataoh, T., Takahashi, H., Shen, H., Suzuki, Y., and Akino, T. (1996) Surfactant protein A accumulating in the alveoli of patients with pulmonary alveolar proteinosis: Oligomeric structure and interaction with lipids, *Am. J. Respir. Cell Mol. Biol.* **14,** 608–619.

Hawgood, S. (1997) Surfactant: Composition, structure and metabolism. *In* Crystal, R. J., and West, J. B. (Eds.), The Lung: Scientific Foundations, 2nd ed., pp. 557–571, Lippincott–Raven, Philadelphia.

Hearn, S. A., and Possmayer, F. (1997) Ultrastructure of tubular myelin in isolated pulmonary surfactant and immunogold labeling of surfactant protein A, *Scanning* **19,** 234–235.

Johansson, J., and Curstedt, T. (1997) Molecular structures and interactions of pulmonary surfactant components, *Eur. J. Biochem.* **244,** 675–693.

Kellenberger, E., Dürrenberger, M., Villiger, W., Carlemam, E., and Wurtz, M. (1987) The efficiency of immunolabel on Lowicryl sections compared to theoretical predictions, *J. Histochem. Cytochem.* **35,** 959–969.

Korfhagen, T. R., Bruno, M. D., Ross, G. F., Huelsman, K. M., Ikegami, M., Jobe, A. H., Wert, S. E., Stripp, B. R., Morris, R. E., Glasser, S., Bachurski, C. J., Iwamoto, H. S., and Whitsett, J. A. (1996) Altered surfactant function and structure in SP-A gene targeted mice, *Proc. Natl. Acad. Sci. USA* **93,** 9594–9599.

Lal, R., and John, S. A. (1994) Biological applications of atomic force microscopy, *Am. J. Physiol.* **35,** 1–21.

Lal, R., and Proksch, R. (1997) Multimodal atomic force microscopy—Biological imaging using atomic force microscopy combined with light fluorescence and confocal microscopies and electrophysiologic recording, *Int. J. Imag. Syst. Tech.* **8,** 293–300.

Manabe, T. (1979) Freeze-fracture study of alveolar lining layer in adult rat lung homogenates, *J. Ultrastruct. Res.* **69,** 86–97.

Possmayer, F. (1988) A proposed nomenclature for pulmonary surfactant-associated proteins, *Am. Rev. Respir. Dis.* **138,** 990–998.

Possmayer, F. (1997) Physicochemical aspects of pulmonary surfactant. *In* Polin, R. A., and Fox, W. W. (Eds.), Fetal and Neonatal Physiology, 2nd ed., pp. 1259–1275, Saunders, Philadelphia.

Poulain, F. R., Allen, A., Williams, M. C., Hamilton, R. L., and Hawgood, S. (1992) Effects of surfactant apoproteins on liposome structure: Implications for tubular myelin formation, *Am. J. Physiol.* **262,** 730–739.

Poulain, F. R., Nir, S., and Hawgood, S. (1996) Kinetics of phospholipid membrane fusion induced by surfactant apoproteins A and B, *Biochim. Biophys. Acta* **1278,** 169–175.

Putman, C. A. J., de Grooth, B. G., Hansma, P. K., van Holst, N. F., and Greve, J. (1993) Immunogold labels: Cell-surface markers in atomic force microscopy, *Ultramicroscopy* **48,** 177–182.

Santos, N. C., Ter-Ovansesyan, E., Zasadzinski, J. A., Prieto, M., and Castanho, M. A. R. B. (1998) Filipin induced lesions in planar phospholipid bilayers imaged by atomic force microscopy, *Biophys. J.* **75,** 1869–1873.

Suzuki, Y., Fujita, Y., and Kogishi, K. (1989) Reconstitution of tubular myelin from synthetic lipids and proteins associated with pig pulmonary surfactant, *Am. Rev. Respir. Dis.* **140,** 75–81.

Ushiki, T., Hittomi, J., Ogura, S., Umemoto, T., and Shigeno, M. (1996) Atomic force microscopy in histology and cytology, *Arch. Histol. Cytol.* **59,** 421–431.

Ushiki, T., Shigeno, M., and Abe, K. (1994) Atomic force microscopy of embedment-free sections of cells and tissues, *Arch. Histol. Cytol.* **57,** 427–432.

Van Golde, L. M. G., Batenburg, J., and Robertson, B. (1994) The pulmonary surfactant system, *News Physiol. Sci.* **9,** 13–20.

Voorhout, W. F., Veenendaal, T., Haagsman, H. P., Verkleij, A., van Golde, L. M. G., and Geuze, H. J. (1991) Surfactant protein A is localized at the corners of the pulmonary tubular myelin lattice, *J. Histochem. Cytochem.* **39,** 1331–1336.

Walker, S. R., Williams, M. C., and Benson, B. (1986) Immunocytochemical localization of the major surfactant apoproteins in type II cells, clara cells and alveolar macrophages of rat lung, *J. Histochem. Cytochem.* **34,** 1137–1148.

Weibel, E. R., and Gil, J. (1968) Electron microscopic demonstration of an extracellular duplex lining layer of the alveoli, *Respir. Physiol.* **4,** 42–57.

Williams, M. C. (1978) Freeze-fracture studies of tubular myelin and lamellar bodies in fetal and adult rat lung, *J. Ultrastruct. Res.* **64,** 352–361.

Williams, M. C., Hawgood, S., and Hamilton, R. L. (1991) Changes in lipid structure produced by surfactant protein SP-A, SP-B and SP-C, *Am. J. Respir. Cell Mol. Biol.* **5,** 41–50.

Yamamoto, A., and Tashiro, Y. (1994) Visualization by an atomic force microscope of the surface of ultra-thin sections of rat kidney and liver cells embedded in LR White, *J. Histochem. Cytochem.* **42,** 1463–1470.

Yamashina, S., and Shigeno, S. (1995) Application of atomic force microscopy to ultrastructural and histochemical studies of fixed and embedded cells, *J. Electron. Microsc.* **44,** 462–466.

Young, S. L., Fram, E. K., and Larson, E. W. (1992) Three-dimensional reconstruction of tubular myelin, *Exp. Lung Res.* **18,** 497–504.

Yu, S., Harding, P. G. R., Smith, N., and Possmayer, F. (1983) Bovine pulmonary surfactant: Chemical composition and physical properties, *Lipids* **18,** 522–529.